Check for updates

A rotational investigation of the three isomeric forms of cyanoethynylbenzene (HCC-C6H4-CN): benchmarking experiments and calculations using the "Lego brick" approach†

Jean-Thibaut Spaniol,[a] Kin Long Kelvin Lee, [ID][b] Olivier Pirali,[a]
Cristina Puzzarini [ID] *[c] and Marie-Aline Martin-Drumel [ID] *[a]

We report the study of three structural isomers of phenylpropiolonitrile (3-phenyl-2-propynenitrile, $C_6H_5-C_3N$) containing an alkyne function and a cyano group, namely *ortho-*, *meta-*, and *para-*cyanoethynylbenzene (HCC$-C_6H_4-$CN). The pure rotational spectra of these species have been recorded at room temperature in the millimeter-wave domain using a chirped-pulse spectrometer (75–110 GHz) and a source-frequency modulation spectrometer (140–220 GHz). Assignments of transitions in the vibrational ground state and several vibrationally excited states were supported by quantum chemical calculations using the so-called "Lego brick" approach [A. Melli, F. Tonolo, V. Barone and C. Puzzarini, J. Phys. Chem. A, 2021, **125**, 9904–9916]. From these assignments, accurate spectroscopic (rotational and centrifugal distortion) constants have been derived: for all species and all observed vibrational states, predicted rotational constants show relative accuracy better than 0.1%, and often of the order of 0.01%, compared to the experimental values. The present work hence further validates the use of the "Lego brick" approach for predicting spectroscopic constants with high precision.

1 Introduction

High performance radio instruments such as the Yebes and Green Bank telescopes or the ALMA and NOEMA observatories are increasing the rate at which the molecular content of astronomical sources is uncovered. Such instruments have enabled about 300 molecules to now be detected in the interstellar medium (ISM), with 20% of them identified in recent years (see, *e.g.*, ref. 1). Because these current interstellar spectral surveys show unprecedented sensitivity and spectral (as well as spacial) resolution, the limiting factor to further interstellar detections—reaching ideally a full knowledge of the interstellar molecular content—is more than ever the availability of high-resolution laboratory spectroscopic data on molecules that could be present in the ISM. With high performance instrumentation now widely available from the microwave to the submillimeter-wave domains, including chirped-pulse and source-frequency

modulation spectrometers,[2,3] recording the rotational spectra of terrestrially stable molecules can now be a matter of days and even down to hours‡. Yet, assigning the high density of the observed spectral lines remains tedious and is very often the limiting factor in the speed of laboratory publications. Hence, several groups are working into means to ease that step, from assisted to automated identification of molecular spectral fingerprints.[4–12] A general census is that reliable, accurate predictions from quantum chemical calculations is a key into speeding up the spectral assignments.[13,14] In this regard, the so-called "Lego brick" approach[14] (also known as TM-SE_LR or TM+LR; *vide infra*), that exploits the idea that the geometry of a molecular system can be built starting from different fragments (the "Lego bricks") whose accurate semi-experimental (SE) equilibrium structures are available, appears extremely promising. Such an approach allows to accurately determine the equilibrium structure of relatively rigid molecules and thus accurately predict their rotational constants. In Melli *et al.*,[14] a compelling benchmarking of the method against, notably, the experimental rotational constants (from Buchanan *et al.*[15]) of phenylpropiolonitrile ($C_6H_5-C_3N$, hereafter PhC3N), was reported. Very recently, the validity of the approach was also verified against the data of

[a] *Université Paris-Saclay, CNRS, Institut des Sciences Moléculaires d'Orsay, 91405 Orsay, France. E-mail: marie-aline.martin@universite-paris-saclay.fr*

[b] *Intel Accelerated Computing Systems and Graphics Group, Intel JF5 2111 NE 25th Ave, Hillsboro, OR 97124, USA*

[c] *Dipartimento di Chimica "Giacomo Ciamician", Università di Bologna, via F. Selmi 2, 40126 Bologna, Italy. E-mail: cristina.puzzarini@unibo.it*

‡ Investigating reactive species on Earth often requires many measurements to obtain spectra with adequate signal-to-noise ratios for analysis which significantly increases the acquisition time.
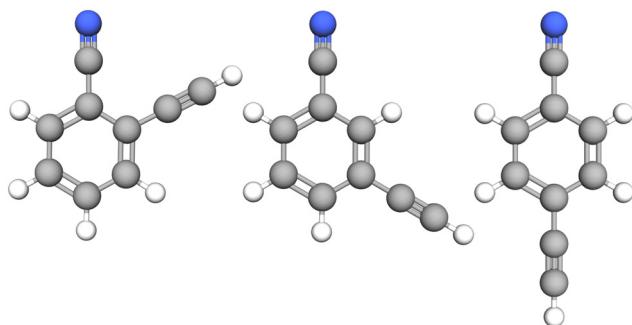
Fig. 1 Molecular structure of the three species investigated in this study: from left to right, *o*-, *m*-, and *p*-cyanoethynylbenzene.

several small-size polycyclic aromatic hydrocarbons (PAHs) and nitrogen-containing PAHs in their ground vibrational states.[16]

The present work results from a combined experimental and theoretical effort to investigate the pure rotational spectra of three molecules of interstellar interest, the *ortho*-, *meta*-, and *para*-cyanoethynylbenzene (or cyanophenylacetylene or ethynyl-benzonitrile, HCC–C₆H₄–CN, Fig. 1)—hereafter *o*-, *m*-, and *p*-CEB—following studies of their PhC₃N isomer.[14,15] CEBs have focused some interest as potential constituents of the ISM as they may be formed by consecutive additions of C₂H and CN (and conversely) to benzene, reactions that have been found—experimentally and theoretically—to be barrierless and exothermic.[17,18] Eventually, *o*-CEB may lead to the formation of nitrogen-containing PAHs which may be of relevance to the chemistry of the atmosphere of Titan.[17,18] With the detection of benzonitrile (C₆H₅–CN) and the recent tentative one of pheny-lacetylene (C₆H₅–C₂H) in TMC-1,[19,20] experimental data on the difunctionalized benzene with –CN and –C₂H become needed. Spectroscopic information on these species is rather scarce and almost entirely focused on *p*-CEB which has been investigated by NMR,[21] UV spectroscopy (in the liquid phase),[22] and whose structure in the solid and crystal phase has been determined.[23] Various complexes of *p*-CEB with water have also been investigated theoretically[24] and by means of infrared-ultraviolet dou-ble resonance.[25,26] Very recently, the reaction of deprotonation of all three CEBs was characterized with electronic structure calculations.[27] Finally, the relative energies of the CEB isomers were calculated in Buchanan *et al.*[15] and their rotational constants were predicted using the "Lego brick" approach in Melli *et al.*[14]

We summarize here our investigations on the three CEB species: their millimeter-wave spectra have been recorded using a chirped-pulse Fourier-transform and a source-frequency modulation spectrometers, and the spectral assignments were supported by quantum chemical calculations performed using the "Lego brick" approach. For each species, pure rotational transitions have been assigned in the ground vibrational state as well as in excited vibrational ones. This work further demonstrates the performances of the "Lego brick" approach to predict the rotational constants of rigid molecules with relative accuracy better than 0.1%.

2 Computational methods

Initial experimental searches were based upon geometry opti-mization calculations carried out at the ωB97X-D/cc-pVQZ level of theory,[28–30] which has previously proven extremely reliable to support experimental assignments of rigid molecules[13] including the PhC₃N isomer of the three CEBs studied in the present work.[15] Details on these calculations, that were performed using the Gaussian 16 suite of electronic structure programs,[31] are reported in Buchanan *et al.*[15] The calculated rotational constants for all three CEB species can be found in Table S1 in the ESI.†

As mentioned in the Introduction, a molecular system can be seen as formed by different fragments (denoted as the "Lego bricks"), whose accurate SE equilibrium geometries are avail-able. The template molecule (TM) approach[32] is then employed to account for the modifications occurring when moving from the isolated fragment to the molecular system considered. The linear regression (LR) model is instead used to correct the linkage between the different fragments.[33,34] The "Lego brick" approach has also been denoted as TM-SE_LR[14] or TM+LR;[16] to keep the notation concise, we will use the latter one (TM+LR) in the following. TM+LR structures for *o*-, *m*-, and *p*-CEBs and a detailed description of the approach are provided in the ESI.†

According to vibrational second-order perturbation theory (VPT2[35]), vibrational ground-state rotational constants (B_0) consist of two terms: the equilibrium part (B_e), which is the largest fraction and only depends on the equilibrium structure and the mass composition, and the vibrational correction (ΔB_{vib}), which requires the computation of the vibration–rotation interaction constants (which—in turn—implies anharmonic force field calculations[36]). In Melli *et al.*,[14] the B_e values of *o*-, *m*-, and *p*-CEB (see Fig. 1) were determined using the TM+LR approach. In that study, the vibration–rotation interaction con-stants were evaluated at the B3LYP-D3/jun-cc-pVDZ level,[37–40] and led to the evaluation of the ΔB_{vib} corrections. In this work, the B3LYP-D3/jun-cc-pVDZ vibration–rotation interaction con-stants have been employed to predict the rotational constants of vibrationally excited states according to the following VPT2 expression:

$$B_{vi} = B_e - \sum_r \alpha_r (v_r + 1/2) = B_0 - \alpha_i \qquad (1)$$

where α_r denotes the vibration–rotation interaction constant for the *r*-th mode and the sum is taken over all fundamental vibra-tional modes *r* (with v_r being the corresponding vibrational quantum number). B_{vi} is the rotational constant of the vibrational state $v_i = 1$ (with *i* being one of the *r* normal modes) and the expression above applies to the three rotational constants (A, B and C). The α_i values are reported in Table S2 in the ESI.† The B3LYP-D3/jun-cc-pVDZ anharmonic force field calculations furthermore allowed the prediction of the low-lying energy levels graphically reported in Fig. 2.

To further support the spectral assignment for the three CEBs studied in this work, their quartic centrifugal distortion constants have been computed using the using Møller-Plesset second-order theory (MP2)[41] in conjunction with the cc-pVTZ

6398 | *Phys. Chem. Chem. Phys.*, 2023, **25**, 6397–6405

This journal is © the Owner Societies 2023
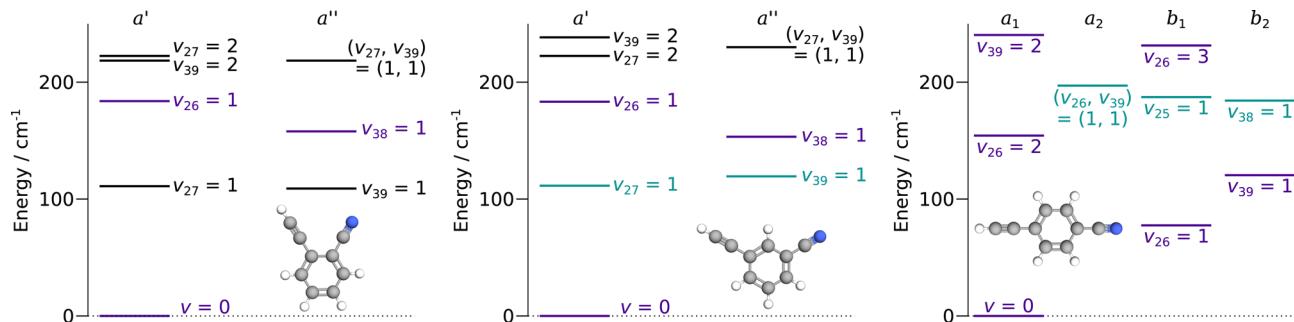
Fig. 2 Lowest energy level diagram of *o*-, *m*-, and *p*-CEB, from left to right, as a function of symmetry. Only states lying below 250 cm^{-1} are represented. Pure rotational transitions within states represented in purple have been assigned in this study. For the states represented in blue-green, tentative assignments are proposed. Energy of states involving several quanta of excitation are obtained by summing the energies of each associated state with a single quantum of excitation.

basis set and within the frozen-core (fc) approximation. This required the evaluation of the harmonic force field, which has been obtained from analytical second-derivative techniques as implemented in the CFOUR quantum-chemistry program.[42,43]

3 Experimental methods

3.1 Samples

The *o*-CEB, *m*-CEB, and *p*-CEB samples, of purity higher than 97%, were purchased from Sigma-Aldrich and used without further purification. All three samples are solid at room temperature but possess sufficient vapor pressure to enable their gas phase investigation.

3.2 Chirped-pulse Fourier-transform millimeter-wave measurements

Measurements in the 75–110 GHz range were performed using a commercial (Brightspec) chirped-pulse (CP) Fourier transform millimeter-wave spectrometer. Vapor pressure, typically of the order of 1.5–2 μbar, of each sample was introduced into a ~60 cm-long cell terminated by two PTFE windows. A slow flow was ensured by a turbomolecular pump (Pfeiffer, HiCube80) to maintain stable pressure conditions during the acquisition and prevent from cell outgassing. Excitation pulses of 0.5, 0.25, and 0.5 μs-length were found to maximize the signal of *o*-, *m*-, and *p*-DCB, respectively. Spectra were recorded in the 75–110 GHz range using the standard High Dynamic Range mode of the instrument which uses a segmented approach with 1165 segments of 30 MHz bandwidth. The final CP spectra are obtained *via* the Fourier-transform of 4 μs of the free induction decay, after applying a Blackman-Harris filter. Under these conditions, isolated transitions of the CEB molecules exhibit a full-width-at-half-maximum (FWHM) of typically 500 kHz (the Doppler-width of the CEB species at 100 GHz is of the order of 100 kHz). For each compound, we acquired spectra averaged over 1 million frames (2 h of acquisition), resulting in a signal-to-noise ratio on the order of ~100 for the strongest transitions.

3.3 Source-frequency modulation millimeter-wave measurements

The spectra of the three species have been recorded in the 140–220 GHz spectral range using a source-frequency modulation

millimeter-wave spectrometer that has been described in detail previously.[15,44] Similarly to the CP measurements, vapor pressure of each sample at room temperature was introduced into a cell at pressure of 1.5–2 μbar and a slow flow—ensured by a turbomolecular pump (Pfeiffer, HiPace350)—was set to prevent from cell outgassing. Here the absorption cell is a 2 m-long/5 cm-diameter Pyrex absorption cell terminated by two 1 cm-thick Teflon windows. The spectrometer combines a microwave synthesizer (2–20 GHz, Rohde & Schwarz) with a frequency multiplication chain (Virginia Diodes Inc., VDI) to generate tunable radiation in the range of interest (from 75 to 900 GHz), modulated in frequency at a modulation frequency of 48.2 kHz. This radiation is collimated by a 10 mm-focal length Teflon lens into the absorption cell before being focused by a second lens (identical to the first one) onto a detector, here a Schottky diode (VDI). The signal is demodulated at the second harmonic by a lock-in amplifier (Ametek). The spectra have been recorded with a 50 kHz frequency step, a 100 ms time constant, and a frequency modulation deviation of 180 kHz. Isolated transitions exhibit a FWHM typically of 400 kHz at 200 GHz, about twice what expected for Doppler-broadened lines. As similarly observed for PhC$_3$N,[15] collisional broadening seems to be significant for these molecules exhibiting a strong permanent dipole moment.

4 Results and discussion

4.1 Spectroscopic considerations

o-CEB and *m*-CEB belong to the C_s point group of symmetry and possess a permanent dipole moment with projections along the *a* axis of 3.9 D and 3.6 D, and along the *b* axis of 2.3 D and 2.5 D, respectively (see the ESI† of Buchanan *et al.*[15]). They possess 39 normal modes of vibration ($\Gamma = 27a' \oplus 12a''$). *p*-CEB belongs to the C_{2v} point group of symmetry and possesses a permanent dipole moment along the *a* axis of 4.3 D. The 39 normal modes of vibration of *p*-CEB follow the irreducible representation $\Gamma = 14a_1 \oplus 3a_2 \oplus 9b_1 \oplus 13b_2$. Owing to two sets of equivalent hydrogen atoms (2 H in *ortho* of the –CCH group and 2 H in *ortho* of the –CN group), the molecule exhibits a statistical weight ratio of 5:3 for *ortho* and *para* levels in the ground

This journal is © the Owner Societies 2023

Phys. Chem. Chem. Phys., 2023, **25**, 6397–6405 | **6399**

vibrational state (a_1 symmetry). For excited states, this ratio is 5 : 3 in states of a_1 or a_2 symmetry, and 3 : 5 in states of b_1 or b_2 symmetry. For the three species, the vibrational states lying below 250 cm^{-1} are represented in Fig. 2. These molecules are asymmetric-top rotors, with Rays asymmetry parameter κ taking values of -0.1, -0.8, and -0.97 for *o*-, *m*-, and *p*-CEB, respectively.

Experimental assignments have been performed using Loomis-Wood diagrams created by the LWWa program for asymmetric top molecules.[45] Rotational constants of all three species have been adjusted using the SPFIT/SPCAT suite of programs;[46] a Watson A-reduced Hamiltonian in the I^r representation has been employed. Simulations of the spectra using the spectroscopic constants have been performed using the PGOPHER software.[47]

4.2 Pure rotational transitions in $v = 0$

For all three species, the assignment of pure rotational transitions within the vibrational ground state was straightforward using predictions derived from the ωB97X-D/cc-pVQZ calculations, and even more obvious using the TM+LR predictions. A comparison of the experimental CP spectrum of *m*-CEB with a simulated spectrum obtained using the predicted TM+LR constants (also incorporating vibrational corrections) from Melli *et al.*,[14] without addition of any centrifugal distortion term, is shown on Fig. 3. The simulation shows clusters visually matching the experimental spectrum (top panel). A zoomed-in view of the first cluster observed in the spectral region covered experimentally (middle panel) reveals that several transitions involving low-K_a values lie very close to the prediction. It is worth noting that *m*-CEB was chosen for illustrating the performances of the TM+LR approach because, out of the three molecules studied in this work, it is the one for which predictions are showing the "worst" agreement with the experiment. Fig. 3 also shows a Loomis-Wood representation of the experimental spectrum around the predictions of the $^QR_0$, $K_a'' + K_c'' = J''$, *a*-type transitions (lower panel). Clear series, colored in blue-green, are visible. These series deviate significantly from the prediction for high J'' values, because no centrifugal distortion effect was taken into account at this stage of the prediction. Nevertheless, the clear progression in K_a'' allows for unambiguous assignments.

In total, thousands of transitions have been assigned to each species. For *o*- and *m*-CEB, both *a*- and *b*-type transitions have been observed, although many of them are overlapping, and many weak Q-branch lines have also been assigned. In total, for these two species, 11 629 and 10 604 transitions have been assigned to 5722 and 6462 different frequencies, respectively. The large difference between number of transitions and number of frequencies comes not only from overlapping *a*- and *b*-type transitions but also from unresolved asymmetric splittings. The range of observed quantum numbers involves up to $J'' = 164$ and $K_a'' = 83$ for *o*-CEB, and $J'' = 167$ and $K_a'' = 76$ for *m*-CEB. Concerning *p*-CEB, for which only *a*-type transitions are allowed, only R-branch transitions have been observed, for a total of 7908 transitions (4814 different frequencies) involving J'' up to 173 and K_a'' up to 56. To derive the spectroscopic constants in $v = 0$
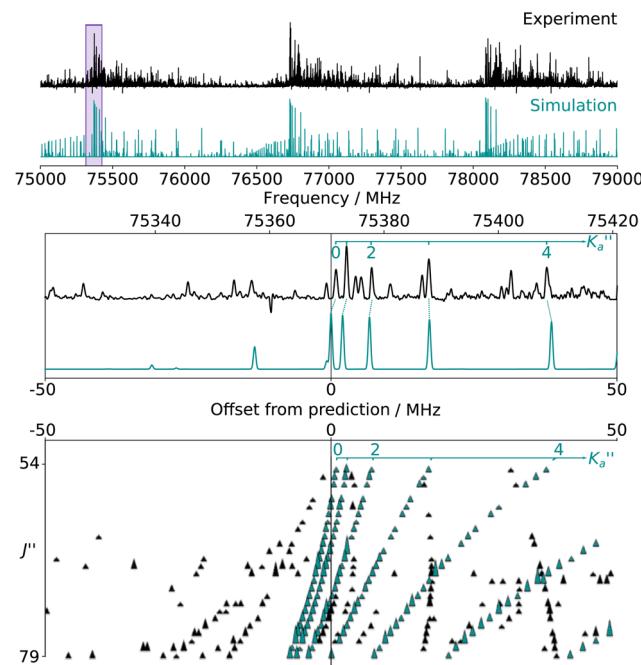
Fig. 3 (Top panel) Portion of the experimental spectrum (in black) of *m*-CEB recorded using the CP spectrometer and comparison with a 300 K simulation performed using the rotational constants predicted by the TM+LR approach (in blue-green). (Middle panel) 100 MHz-wide zoom around the predicted frequency of the $J'_{K_a',K_c'} - J''_{K_a'',K_c''} = 55_{0,55} - 54_{0,54}$ transition; the corresponding spectral window is highlighted by a purple area on the top panel. (Bottom panel) Loomis-Wood plot for the $^QR_0$, $K_a'' + K_c'' = J''$, *a*-type transitions where each experimental transition is represented by a triangle of height proportional to its intensity. Each horizontal section is a 100 MHz-wide portion of the spectrum around the prediction of the corresponding J'' transition, hence the $J'' = 54$ segment matches the zoom presented in the middle panel while the $J'' = 79$ one corresponds to the highest frequency cluster visible in the top panel. For the sake of clarity, weak transitions, as well as the 140–220 GHz range, are not represented. Lines assigned to transitions involving the aforementioned selection rule are shown in blue-green. The $K_a = 0$–5 series are labeled in blue-green in both the middle and bottom panels.

for the three species, all transitions were weighted according to their expected experimental accuracy, assumed here to be 50 kHz. To reproduce the data to this experimental accuracy, inclusion of quartic and sextic centrifugal distortion constants was required. In that regard, the assignment of transitions in the 140–220 GHz range (not represented in Fig. 3), involving high J values, was crucial. Table 1 summarizes the derived rotational constants and the centrifugal distortion ones and Table 2 the relevant fit parameters. Overall, the three fits are quite satisfactory and take root mean square (RMS) values of 47 kHz, 45 kHz, and 37 kHz (hence weighted standard deviations of 0.94, 0.91, and 0.73) for *o*-, *m*-, and *p*-CEB, respectively. It is worth noting that for *p*-CEB, since $A \gg B \sim C$, a fit in the *S*-reduction was also performed. The only parameter affected by this change is δ_K and overall the resulting fit is of similar quality, taking the same RMS and weighted standard deviation values, as using the *A*-reduction.

Table 1 allows for a comparison of the experimentally-derived rotational constants in $v = 0$ with those predicted using the TM+LR approach reported in Melli *et al.*[14] The agreement is

6400 | *Phys. Chem. Chem. Phys.*, 2023, **25**, 6397–6405

This journal is © the Owner Societies 2023

Table 1 Rotational constants of *o*-, *m*-, and *p*-CEB in the ground and singly excited vibrational states; comparison with predictions from the TM+LR approach. Quartic centrifugal distortion constants are reported in $v = 0$ and compared to equilibrium values calculated at the fc-MP2/cc-pVTZ level of theory (for higher order parameters and values derived in the excited vibrational states, see Table 2)

Parameter		*o*-CEB			*m*-CEB			*p*-CEB		
		Exp./MHz	Pred.[a]/MHz	Diff.[b]/%	Exp./MHz	Pred.[a]/MHz	Diff.[b]/%	Exp./MHz	Pred.[a]/MHz	Diff.[b]/%
$v = 0$	A	2027.441205 (98)	2028.34	0.04	2704.87469 (15)	2707.11	0.08	5646.3543 (52)	5647.34	0.02
	B	1329.456144 (39)	1329.37	<0.01	907.033894 (26)	906.69	0.04	709.161497 (30)	709.10	0.01
	C	802.668552 (30)	802.78	0.01	679.066023 (24)	679.01	0.01	630.029790 (29)	629.98	0.01
	$\Delta_J \times 10^3$	0.0721681 (56)	0.0715	0.9	0.0419596 (16)	0.0418	0.4	0.00795215 (46)	0.00766	3.8
	$\Delta_{JK} \times 10^3$	−0.399792 (18)	−0.409	2.3	−0.434212 (11)	−0.442	1.8	0.145379 (14)	0.146	0.4
	$\Delta_K \times 10^3$	1.815892 (62)	1.90	4.4	2.63191 (19)	2.66	1.1	1.134 (17)	1.08	5.0
	$\delta_J \times 10^3$	0.0302466 (26)	0.0299	1.2	0.01709415 (89)	0.0171	<0.1	0.00107654 (28)	0.00105	2.5
	$\delta_K \times 10^3$	−0.0630206 (99)	−0.0682	7.6	0.0593386 (74)	0.0562	5.6	0.119902 (99)	0.120	0.1
$v_{38} = 1$	E^c		158			153				
	A	2014.2218 (80)	2014.11	<0.01	2684.948 (33)	2687.42	0.09			
	B	1330.7245 (42)	1330.73	<0.01	907.7190 (39)	907.68	<0.01			
	C	803.548695 (94)	803.46	0.01	679.680020 (99)	679.65	<0.01			
$v_{26} = 1$	E^c		184			183			77	
	A	2042.9632 (12)	2042.28	0.03	2727.459 (27)	2724.70	0.10	5541.7655 (67)	5547.27	0.10
	B	1331.82713 (51)	1331.82	<0.01	908.3147 (32)	908.26	<0.01	709.636066 (40)	709.63	<0.01
	C	803.15419 (12)	803.09	0.01	679.466887 (93)	679.43	<0.01	630.790167 (37)	630.75	<0.01
$v_{39} = 1$	E^c								120	
	A							5746.7343 (78)	5741.47	0.09
	B							709.824720 (46)	709.79	<0.01
	C							630.327283 (42)	630.30	<0.01

[a] For A, B, C: in $v = 0$, Pred. = calc.; otherwise, Pred. = Exp.$(v = 0) - \alpha_{i\text{calc}}$. *[b]* |(Exp. − calc.)/calc.| × 100. *[c]* cm^{-1}.

excellent, with absolute relative differences better than 0.1% and often of the order of 0.01%. In comparison, the predictions obtained by Bayesian scaling of the equilibrium constants using the method described in Lee and McCarthy *et al.*[13] (Table S6 of Buchanan *et al.*[15]) show marginally worse agreement with the experimental values, with absolute relative differences of the order of 0.5% or better (see Table S1 in the ESI†). Such agreement is particularly fair with respect to the relatively low computational cost of this approach where no vibrational corrections have to be calculated because a statistical correction in lieu of them is assumed. Finally, it is worth noting that the scaled predictions using the rotational constants of the PhC$_3$N isomer (also proposed in the Table S6 of Buchanan *et al.*[15] and reported in Table S1 in the ESI†) brings that difference down to better 0.05% for B and C, although the error on A remains larger (especially for *o*-CEB, see Table S1, ESI†). This last method, however, remains only applicable within an isomeric family and implies that one isomer has already been observed experimentally, and does not reach the level of accuracy achieved by the TM+LR approach. Concerning the quartic centrifugal distortion constants, for all three species, the values derived in $v = 0$ from the fits are in excellent agreement with the MP2 computed values, both in sign and order of magnitude (see Table 1), with averaged deviations of ~3%. In particular, for *p*-CEB, even though only *a*-type transitions are observed, the Δ_K parameter is accurately determined (although not at the level reached for the other species). The comparison of experiment with B3LYP-D3/jun-cc-pVDZ quartic centrifugal distortion constants is presented and discussed in

the ESI.† This points out potential problems in the Gaussian 16 package.

Fits of these data using a Watson Hamiltonian in the III^r representation were also attempted with the PGOPHER software. In all cases, these fits were not as satisfactory as using the I^r representation (larger weighted standard deviation, requirement of inclusion of higher order centrifugal distortion parameters to reproduce data at their experimental accuracy) and, in the case of *o*-CEB, no proper fit was achieved at all. We conclude that the I^r representation is more suited than the III^r one to reproduce the data of the CEB species.

4.3 Pure rotational transitions within the vibrationally excited states

The numerous low-lying vibrational states of each species possess significant population at room temperature which results in a high density of lines with significant intensity visible on the experimental spectra. To search for pure rotational transitions within the vibrationally excited states involving one quantum of excitation, predictions were obtained by subtracting the calculated vibration–rotation interaction constant α (see Table S2 in the ESI†) to the experimental rotational constants in $v = 0$ for each species (in eqn (1), the experimental B_0 is thus used). The corresponding predicted rotational constants are reported in Table 1. To account for centrifugal distortion, values derived for the quartic and sextic constants in $v = 0$ (see Table 2) were used as a starting point. Using these predictions, spectral attributions are, again, straightforward for several vibrational states. An example, the case of $v_{38} = 1$ for *o*-

Paper

Table 2 Centrifugal distortion constants of o-, m-, and p-CEB in the ground and singly excited vibrational states observed in this study. Values in parentheses are errors (1σ) in the unit of the last digit. Parameters without an error are fixed (to the value in v = 0)

Parameter[a]	o-CEB			m-CEB			p-CEB		
	$v = 0$	$v_{38} = 1$	$v_{26} = 1$	$v = 0$	$v_{38} = 1$	$v_{26} = 1$	$v = 0$	$v_{26} = 1$	$v_{39} = 1$
$\Delta_J \times 10^3$	0.0721681 (56)	0.0717 (10)	0.071626 (55)	0.0415596 (16)	0.04399 (51)	0.04218 (23)	0.00795215 (46)	0.00805657 (61)	0.00800410 (71)
$\Delta_{JK} \times 10^3$	-0.399792 (18)	-0.566 (36)	-0.4950 (12)	-0.434212 (11)	-0.3892 (95)	-0.5191 (44)	0.145379 (14)	0.143217 (23)	0.144134 (35)
$\Delta_K \times 10^3$	1.815892 (62)	1.89 (11)	2.4420 (40)	2.63191 (19)	1.067 (34)	4.022 (17)	1.134 (17)	-7.538 (22)	9.869 (26)
$\delta_J \times 10^3$	0.0302466 (26)	0.03001 (52)	0.030009 (29)	0.0170415 (89)	0.01808 (25)	0.01722 (12)	0.00107654 (28)	0.00105418 (37)	0.00110228 (43)
$\delta_K \times 10^3$	-0.0630206 (99)	-0.198 (20)	-0.06348 (67)	0.0593386 (74)	0.0593386	0.0593386	0.119902 (99)	0.01888 (13)	0.21333 (15)
$\Phi_J \times 10^9$	0.05730 (40)	0.05730	0.05730	0.023560 (48)	0.02327 (13)	0.02366 (11)	0.05162 (26)	0.07957 (48)	0.01844 (71)
$\Phi_{JK} \times 10^9$	-0.6072 (12)	-1.303 (18)	-0.0485 (65)	-0.28178 (80)	-0.28178	-0.28178	-0.9319 (44)	-0.7494 (89)	-1.103 (15)
$\Phi_{KJ} \times 10^9$	1.2633 (44)	1.2633	-8.156 (47)	0.4892 (34)	0.4892	0.4892			
$\Phi_K \times 10^9$	1.866 (12)	-12.24 (30)	32.54 (21)	5.017 (71)	5.017	5.017			
$\phi_J \times 10^9$	0.02875 (20)	0.02875	0.02794 (18)	0.011514 (29)	0.011514	0.011514			
$\phi_{JK} \times 10^9$	-0.1692 (12)	-0.1692	-0.1692						
$\phi_K \times 10^9$	1.2930 (16)	-4.41 (11)	1.2930	2.1395 (79)	2.1395	2.1395			
N/n^b	11 629/5722	2785/1492	3043/1717	10604/6462	2063/1068	1843/1064	7908/4814	6316/3951	5442/6474
$J''_{max}, K''_{a\,max}$	164, 83	135, 30	135, 37	167, 76	159, 20	160, 22	173, 56	172, 49	173, 45
RMS^c	0.047	0.075	0.072	0.045	0.065	0.067	0.037	0.047	0.051
σ^d	0.94	1.01	0.96	0.91	0.87	0.89	0.73	0.93	1.01

[a] In MHz, unless otherwise noted. [b] Number of lines (N) and number of lines with different frequencies (n), unitless. [c] Root mean square, in MHz. [d] Weighted standard deviation, unitless.

CEB, is presented on Fig. 4 (in orange). On this figure, showing the first cluster of lines visible in the CP spectrum, the series of transitions in $v_{38} = 1$ appear well predicted, down to the band head at $K''_a = 5 - 6$, and merely shifted by 8 MHz or less from the experimental observation. It is interesting to note that extrapolation of the K''_a series in the Loomis-Wood plot to $J'' = 0$ would bring the $K''_a = 0$ series to a 0 MHz offset value, a further assessment of the quality of the prediction.

Overall, we assigned for each molecule pure rotational transitions within two vibrationally excited states involving a single quantum of excitation, namely $v_{38} = 1$ (a'' symmetry, 158 cm^{-1}) and $v_{26} = 1$ (a' symmetry, 184 cm^{-1}) for o-CEB, $v_{38} = 1$ (a'', 153 cm^{-1}) and $v_{26} = 1$ (a', 183 cm^{-1}) for m-CEB, and $v_{26} = 1$ (b_1, 77 cm^{-1}) and $v_{29} = 1$ (b_2, 120 cm^{-1}) for p-CEB (see Fig. 2 for a graphical representation; energy values are at the B3LYP-D3/jun-cc-pVDZ level). For each of these, a thousand or more different frequencies have been assigned with J'' quantum numbers spanning a similar range to those involving $v = 0$ and K''_a up to at least 20 (the lower in energy is the level, the higher K''_a values have been assigned). A detailed account on the assignments is reported in Table 2. Spectroscopic constants
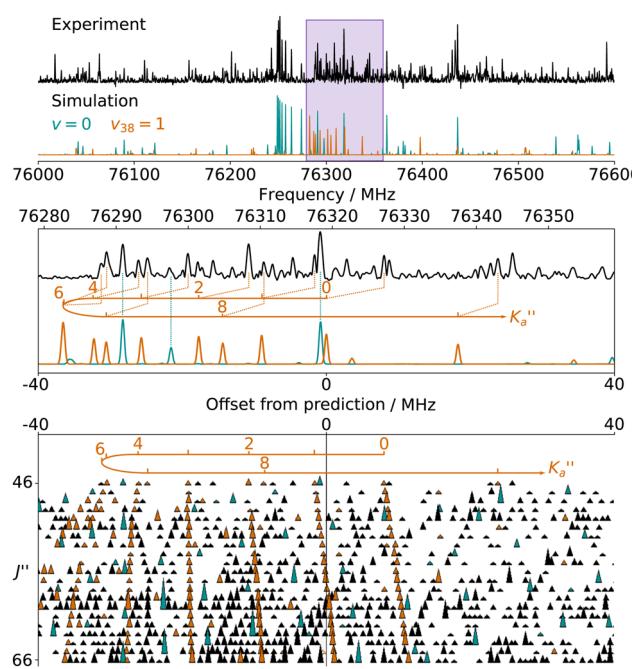

Fig. 4 (Top panel) Portion of the experimental spectrum around 76 GHz (in black) of o-CEB recorded using the CP spectrometer and comparison with a 300 K simulation of the spectrum in the vibrational ground state (in blue-green) and in $v_{38} = 1$ (in orange). The $v = 0$ simulation was performed using the final set of spectroscopic constants while the one in $v_{38} = 1$ was obtained using the rotational constants predicted using eqn (1) (with the experimental B_0). (Middle Panel) 80 MHz-wide zoom around the predicted frequency of the $J'_{K'_a,K'_c} - J''_{K''_a,K''_c} = 47_{0,47} - 46_{0,46}$ transition; the corresponding spectral window is highlighted by a purple area on the top panel. (Bottom panel) Loomis-Wood plot for the $^QR_0$, $K''_a + K''_c = J''$, a-type transitions with 80 MHz-wide segments, similar to the plot presented in Fig. 3. Lines assigned to transitions in $v = 0$ are shown in blue-green, those in $v_{38} = 1$ in orange. The $K_a = 0–9$ series in $v_{38} = 1$ are labeled in orange.

6402 | *Phys. Chem. Chem. Phys.*, 2023, **25**, 6397–6405

This journal is © the Owner Societies 2023

for each set of data have been adjusted using a similar Hamiltonian to that for the ground vibrational state of each molecule and all transitions have been weighted to their experimental accuracy, assumed to be 75 kHz for the two observed vibrational satellites of o- and m-CEB, and 50 kHz for those of p-CEB (based on the signal-to-noise ratio of these features). The smaller value for p-CEB arises from the stronger intensities of these satellites (which results from the fact that the corresponding vibrational states lie relatively low in energy). The resulting sets of parameters are reported in Tables 1 and 2. All fits take a weighted standard deviation close to unity. The agreement between the experimentally derived rotational constants and those predicted is again excellent, with all absolute relative difference better than 0.1%. The B and C constants are often predicted within 0.01%. We note that the Δ_K values in the vibrationally excited states of p-CEB are significantly different from the ground state value. A fit with Δ_K fixed to the ground state (or the calculated) value did not allow to reproduce the transitions satisfactorily and no other distortion parameter, including higher order ones, enabled a proper fit of the data. Such wide variations in Δ_K may arise from some perturbations in these excited states.

Each of the three species possesses two additional vibrational states involving a single quantum of excitation lying below 250 cm^{-1}: $\nu_{39} = 1$ (a'' symmetry, 109 cm^{-1}) and $\nu_{27} = 1$ (a' symmetry, 111 cm^{-1}) for o-CEB, $\nu_{27} = 1$ (a', 111 cm^{-1}) and $\nu_{39} = 1$ (a'', 119 cm^{-1}) for m-CEB, and $\nu_{38} = 1$ (b_2, 184 cm^{-1}) and $\nu_{25} = 1$ (b_1, 187 cm^{-1}) for p-CEB (see Fig. 2). For o- and m-CEB, these states lie at lower energy than those for which we report spectroscopic assignments and indeed strong transitions are seen in the vicinity of the predictions. The spectra, however, appear severely perturbed. At this stage, it has not been possible to assign and fit with confidence the transitions within these vibrational states that lie very close in energy. Tentative assignments are proposed for $\nu_{27} = 1$ and $\nu_{39} = 1$ for m-CEB, and $\nu_{38} = 1$ and $\nu_{25} = 1$ for p-CEB (these states are shown in blue-green in Fig. 2). In each case, only a few K_a series that appeared the least perturbed have been assigned. The derived tentative spectroscopic constants are reported in Tables S3 and S4 in the ESI.† The experimentally-derived B and C rotational constants appear in excellent agreement with the predictions (to better than 0.1%). The A constant, however, is not as close (with about 2% difference for m-CEB) which may be attributed to the fact that the current model does not attempt to treat the interaction between the energy levels. No assignment was possible for $\nu_{39} = 1$ and $\nu_{27} = 1$ of o-CEB, maybe because these vibrational states are calculated to lie the closest in energy, and thus may suffer the most from perturbations.

Finally, for p-CEB we have also assigned pure rotational transitions within vibrational states involving several quanta of excitation: $\nu_{26} = 2$ (a_1 symmetry, 154 cm^{-1}), $\nu_{26} = 3$ (b_1, 231 cm^{-1}), and $\nu_{39} = 2$ (a_1, 240 cm^{-1}). Predictions for these states were performed using experimental α values derived from the analysis of the lower vibrational states using eqn (1). As expected from such purely experimental scaling, the predictions were extremely close to the experimental transitions. About 2000 different frequencies were assigned to each of these vibrational states, and the spectroscopic constants resulting from the fit of these

data are presented in Table S5 in the ESI.† Transitions within $\nu_{26} = 2$ were given a 50 kHz uncertainty and those in $\nu_{26} = 3$ and $\nu_{39} = 2$ a 75 kHz one. All fit have a weighted standard deviation close to unity. The experimentally-derived B and C values are almost equal to the predicted ones (with differences lower than 0.0004%) while A constants are within 0.1% of the prediction. Assignments are also proposed within the $(\nu_{26}, \nu_{39}) = (1,1)$ vibrational state, although they remain tentative as this vibrational energy state lies very close to $\nu_{38} = 1$ and $\nu_{25} = 1$ (Fig. 2), and appears severely perturbed as well. The corresponding spectroscopic constants and preliminary fit parameters are reported in Table S4 in the ESI.† For these three states, as well as the two perturbed ones for o- and m-CEB, a proper study of the interaction between the energy levels lying close in energy appears mandatory to enable secure assignments of the full bands and derive accurate spectroscopic constants. Fig. 5 presents a portion of the spectrum, around 218 GHz, recorded for the p-CEB molecule using the source-frequency modulation spectrometer and a comparison with the simulations of the pure rotational transitions within the vibrational ground state and the five vibrationally-excited states assigned with confidence in this study. Because the models for $\nu_{38} = 1$, $\nu_{25} = 1$, and $(\nu_{26}, \nu_{39}) = (1,1)$ are not reliable at this stage, the corresponding transitions are not represented on the Figure, although they should be stronger than those within $\nu_{26} = 3$. Regardless, the spectral density of the p-CEB spectrum is nicely reproduced by the simulation and the remaining transitions (at the exclusion of those in the three perturbed states mentioned above) are quite weak. It is also worth to mention that pure rotational transitions of isotopic
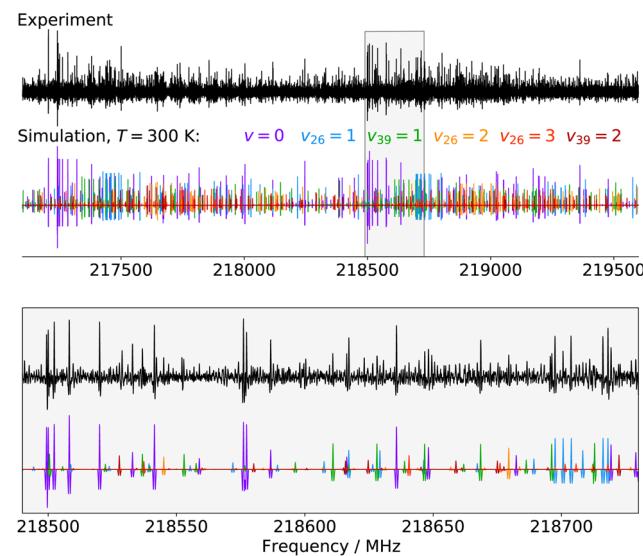
Fig. 5 Portions of the spectrum of p-CEB recorded in this work using the source-frequency modulation millimeter-wave spectrometer and comparison with simulations (at 300 K) of the pure rotational spectrum of the molecule in the six vibrational states assigned in this study (from $v = 0$ to $\nu_{39} = 2$ by increasing energy, see Fig. 2). The second derivative of the simulations is plotted, for better comparison with the experimental spectrum. The lower panel is a zoom-in on the region highlighted in gray in the upper panel.

This journal is © the Owner Societies 2023

Phys. Chem. Chem. Phys., 2023, **25**, 6397–6405 | **6403**

variants of the species also contribute to the spectral density, although these transitions exhibit at most 1% of the intensity of those of the main species in $\nu = 0$.

For all three species and all observed vibrational states, the lists of experimental assignments (secured and tentative) and all fit files are provided in the ESI,† as ASCII files.

4.4 Astronomical implications

Since both –CN and –C_2H are strongly polar groups, and since chemically similar species benzonitrile and phenylacetylene are known (or very likely) interstellar molecules,[19,20] each CEB isomer is a strong candidate for interstellar detection, and the spectroscopic data obtained throughout this study enables astronomical searches for these molecules. Conditions relevant to likely environments are dark molecular clouds and objects along the star formation process—such as Serpens 1a—where benzonitrile has been detected. More relevant to the vibrationally excited states reported here are warm carbon chemistry regions and hot corinos that possess significantly higher (~ 100 K) gas temperatures[48] which facilitate population of these states, barring dynamic effects such as pumping or state–specific formation.

Regarding astrochemical dynamics, detection of any of these isomers and their relative ratios would provide a wealth of information: among molecular families currently detected in the ISM, these o/m/p-CEB isomers should—under terrestrial conditions—demonstrate preferences to either $ortho$/$para$ or $meta$ direction depending on the sequence of reactions. If CEB is formed via addition of –C_2H to benzonitrile, –CN is known to be $meta$ directing based on Hirshfeld charges,[49] whereas –CN addition to phenylacetylene would likely be $ortho$/$para$-directing. By quantifying the relative abundance of each isomer, we would be able to infer the mechanistic history of this isomeric family, whether it is dominated by thermodynamics or kinetics, and ultimately gain invaluable insight into the validity of chemical models.

5 Conclusions

In this study we have exploited the "Lego brick" (also known as TM-SE_LR or TM+LR) approach to assign the pure rotational spectrum of three molecules—o-CEB, m-CEB, and p-CEB—in their vibrational ground state and several vibrationally excited states. The performances of the TM+LR approach are excellent, enabling spectroscopic assignments of these rather rigid molecules in a matter of hours for the vibrational ground state, making this analysis step competitive in time with the spectral acquisition and calculation time (both of which are also a matter of hours). The present work further confirms previous results obtained using this approach.[14,16] Beyond benchmarking of the "Lego brick" approach, the accurate spectroscopic parameters derived for each molecule enable their searches in various interstellar environments, at any temperature down from 300 K, though observations at frequencies up to, reliably, 220 GHz.

Conflicts of interest

There are no conflicts to declare.

Notes and references

1 D. E. Woon, A hyper-bibliography of known astromolecules, http://www.astrochymist.org/.

2 G. G. Brown, B. C. Dian, K. O. Douglass, S. M. Geyer, S. T. Shipman and B. H. Pate, *Rev. Sci. Instrum.*, 2008, **79**, 053103.

3 S. L. Widicus Weaver, *Annu. Rev. Astron. Astrophys.*, 2019, **57**, 79–112.

4 K. N. Crabtree, M.-A. Martin-Drumel, G. G. Brown, S. A. Gaster, T. M. Hall and M. C. McCarthy, *J. Chem. Phys.*, 2016, **144**, 124201.

5 M.-A. Martin-Drumel, M. C. McCarthy, D. Patterson, B. A. McGuire and K. N. Crabtree, *J. Chem. Phys.*, 2016, **144**, 124202.

6 M. Martin-Drumel, C. Endres, O. Zingsheim, T. Salomon, J. van Wijngaarden, O. Pirali, S. Gruet, F. Lewen, S. Schlemmer, M. McCarthy and S. Thorwirth, *J. Mol. Spectrosc.*, 2015, **315**, 72–79.

7 O. Zingsheim, L. Bonah, F. Lewen, S. Thorwirth, H. S. Müller and S. Schlemmer, *J. Mol. Spectrosc.*, 2021, **381**, 111519.

8 L. Bonah, O. Zingsheim, H. S. Müller, J.-C. Guillemin, F. Lewen and S. Schlemmer, *J. Mol. Spectrosc.*, 2022, **388**, 111674.

9 N. A. Seifert, I. A. Finneran, C. Perez, D. P. Zaleski, J. L. Neill, A. L. Steber, R. D. Suenram, A. Lesarri, S. T. Shipman and B. H. Pate, *J. Mol. Spectrosc.*, 2015, **312**, 13–21.

10 W. L. Meerts and M. Schmitt, *Int. Rev. Phys. Chem.*, 2006, **25**, 353–406.

6404 | *Phys. Chem. Chem. Phys.*, 2023, **25**, 6397–6405

This journal is © the Owner Societies 2023

11 M. McCarthy and K. L. K. Lee, *J. Phys. Chem. A*, 2020, **124**, 3002–3017.

12 M. C. McCarthy, K. L. K. Lee, P. B. Carroll, J. P. Porterfield, P. B. Changala, J. H. Thorpe and J. F. Stanton, *J. Phys. Chem. A*, 2020, **124**, 5170–5181.

13 K. L. K. Lee and M. McCarthy, *J. Phys. Chem. A*, 2020, **124**, 898–910.

14 A. Melli, F. Tonolo, V. Barone and C. Puzzarini, *J. Phys. Chem. A*, 2021, **125**, 9904–9916.

15 Z. Buchanan, K. L. K. Lee, O. Chitarra, M. C. McCarthy, O. Pirali and M.-A. Martin-Drumel, *J. Mol. Spectrosc.*, 2021, **377**, 111425.

16 H. Ye, S. Alessandrini, M. Melosso and C. Puzzarini, *Phys. Chem. Chem. Phys.*, 2022, **24**, 23254–23264.

17 A. Landera and A. M. Mebel, *Faraday Discuss.*, 2010, **147**, 479.

18 C. J. Bennett, S. B. Morales, S. D. Le Picard, A. Canosa, I. R. Sims, Y. H. Shih, A. H. H. Chang, X. Gu, F. Zhang and R. I. Kaiser, *Phys. Chem. Chem. Phys.*, 2010, **12**, 8737.

19 B. A. McGuire, A. M. Burkhardt, S. Kalenskii, C. N. Shingledecker, A. J. Remijan, E. Herbst and M. C. McCarthy, *Science*, 2018, **359**, 202–205.

20 J. Cernicharo, M. Agúndez, R. I. Kaiser, C. Cabezas, B. Tercero, N. Marcelino, J. R. Pardo and P. de Vicente, *Astron. Astrophys.*, 2021, **655**, L1.

21 D. A. Dawson and W. F. Reynolds, *Can. J. Chem.*, 1975, **53**, 373–382.

22 X.-K. Jiang, G.-Z. Ji, D. Z.-R. Wang and J. R.-Y. Xie, *J. Phys. Org. Chem.*, 1995, **8**, 781–790.

23 S. Mahapatra, Y. Azim and G. R. Desiraju, *J. Mol. Struct.*, 2010, **976**, 200–204.

24 A. Masunov and J. Dannenberg, *J. Mol. Struct.: THEOCHEM*, 1996, **371**, 17–19.

25 S. Maity and G. N. Patwari, *J. Phys. Chem. A*, 2010, **114**, 8337–8344.

26 S. Maity and G. Naresh Patwari, *Indian J. Phys.*, 2012, **86**, 173–179.

27 M. E. Strauss, T. J. Santaloci and R. C. Fortenberry, *Chemistry*, 2022, **4**, 42–56.

28 J.-D. Chai and M. Head-Gordon, *Phys. Chem. Chem. Phys.*, 2008, **10**, 6615.

29 T. H. Dunning, *J. Chem. Phys.*, 1989, **90**, 1007–1023.

30 D. E. Woon and T. H. Dunning, *J. Chem. Phys.*, 1993, **98**, 1358–1371.

31 M. J. Frisch, G. W. Trucks, H. B. Schlegel, G. E. Scuseria, M. A. Robb, J. R. Cheeseman, G. Scalmani, V. Barone, G. A. Petersson, H. Nakatsuji, X. Li, M. Caricato, A. V. Marenich, J. Bloino, B. G. Janesko, R. Gomperts, B. Mennucci, H. P. Hratchian, J. V. Ortiz, A. F. Izmaylov, J. L. Sonnenberg, D. Williams-Young, F. Ding, F. Lipparini, F. Egidi, J. Goings, B. Peng, A. Petrone, T. Henderson, D. Ranasinghe, V. G. Zakrzewski, J. Gao, N. Rega, G. Zheng, W. Liang, M. Hada, M. Ehara, K. Toyota, R. Fukuda, J. Hasegawa, M. Ishida, T. Nakajima, Y. Honda, O. Kitao, H. Nakai, T. Vreven, K. Throssell,

J. A. Montgomery, Jr., J. E. Peralta, F. Ogliaro, M. J. Bearpark, J. J. Heyd, E. N. Brothers, K. N. Kudin, V. N. Staroverov, T. A. Keith, R. Kobayashi, J. Normand, K. Raghavachari, A. P. Rendell, J. C. Burant, S. S. Iyengar, J. Tomasi, M. Cossi, J. M. Millam, M. Klene, C. Adamo, R. Cammi, J. W. Ochterski, R. L. Martin, K. Morokuma, O. Farkas, J. B. Foresman and D. J. Fox, *Gaussian 16 Revision A.01*, 2016.

32 M. Piccardo, E. Penocchio, C. Puzzarini, M. Biczysko and V. Barone, *J. Phys. Chem. A*, 2015, **119**, 2058–2082.

33 E. Penocchio, M. Piccardo and V. Barone, *J. Chem. Theory Comput.*, 2015, **11**, 4689–4707.

34 G. Ceselin, V. Barone and N. Tasinato, *J. Chem. Theory Comput.*, 2021, **17**, 7290–7311.

35 I. Mills, in *Molecular spectroscopy: modern research*, ed. K. N. Rao and C. W. Matthews, Academic Press, 1972, pp. 115–140.

36 C. Puzzarini, J. F. Stanton and J. Gauss, *Int. Rev. Phys. Chem.*, 2010, **29**, 273–367.

37 A. D. Becke, *Phys. Rev. A*, 1988, **38**, 3098–3100.

38 C. Lee, W. Yang and R. G. Parr, *Phys. Rev. B: Condens. Matter Mater. Phys.*, 1988, **37**, 785–789.

39 S. Grimme, J. Antony, S. Ehrlich and H. Krieg, *J. Chem. Phys.*, 2010, **132**, 154104.

40 E. Papajak and D. G. Truhlar, *J. Chem. Theory Comput.*, 2011, **7**, 10–18.

41 C. Møller and M. S. Plesset, *Phys. Rev.*, 1934, **46**, 618–622.

42 J. F. Stanton, J. Gauss, L. Cheng, M. E. Harding, D. A. Matthews and P. G. Szalay with contributions from A. A. Auer, R. J. Bartlett, U. Benedikt, C. Berger, D. E. Bernholdt, Y. J. Bomble, O. Christiansen, F. Engel, R. Faber, M. Heckert, O. Heun, M. Hilgenberg, C. Huber, T.-C. Jagau, D. Jonsson, J. Jusélius, T. Kirsch, K. Klein, W. J. Lauderdale, F. Lipparini, T. Metzroth, L. A. Mück, D. P. O'Neill, D. R. Price, E. Prochnow, C. Puzzarini, K. Ruud, F. Schiffmann, W. Schwalbach, C. Simmons, S. Stopkowicz, A. Tajti, J. Vázquez, F. Wang, J. D. Watts and the integral packages MOLECULE (J. Almlöf and P.R. Taylor), PROPS (P.R. Taylor), ABACUS (T. Helgaker, H.J. Aa. Jensen, P. Jørgensen, and J. Olsen), and ECP routines by A. V. Mitin and C. van Wüllen, *CFOUR, a quantum chemical program package*, 2016, see http://www.cfour.de.

43 D. A. Matthews, L. Cheng, M. E. Harding, F. Lipparini, S. Stopkowicz, T.-C. Jagau, P. G. Szalay, J. Gauss and J. F. Stanton, *J. Chem. Phys.*, 2020, **152**, 214108.

44 O. Pirali, M. Goubet, V. Boudon, L. D'Accolti, C. Fusco and C. Annese, *J. Mol. Spectrosc.*, 2017, **338**, 6–14.

45 W. Łodyga, M. Kręglewski, P. Pracna and Š. Urban, *J. Mol. Spectrosc.*, 2007, **243**, 182–188.

46 H. M. Pickett, *J. Mol. Spectrosc.*, 1991, **148**, 371–377.

47 C. M. Western, *J. Quant. Spectrosc. Radiat. Transfer*, 2017, **186**, 221–242.

48 J. Kalvāns, *Astrophys. J.*, 2021, **910**, 54.

49 S. Liu, *J. Chem. Phys.*, 2014, **141**, 194109.

This journal is © the Owner Societies 2023

Phys. Chem. Chem. Phys., 2023, **25**, 6397–6405 | **6405**